Inorganic Chemistry

Article

pubs.acs.org/IC

Trigonal Mn_3 and Co_3 Clusters Supported by Weak-Field Ligands: A Structural, Spectroscopic, Magnetic, and Computational Investigation into the Correlation of Molecular and Electronic Structure

Alison R. Fout, Dianne J. Xiao, Qinliang Zhao, T. David Harris, Evan R. King, Emily V. Eames, Shao-Liang Zheng, and Theodore A. Betley*

Department of Chemistry and Chemical Biology, Harvard University, 12 Oxford Street Cambridge, Massachusetts 02138, United States

Supporting Information

ABSTRACT: Transamination of divalent transition metal starting materials ($M_2(N(SiMe_3)_2)_4$, M = Mn, Co) with hexadentate ligand platforms $^{R}LH_6$ ($^{R}LH_6$ = $MeC(CH_2NPh\text{-}o\text{-}NR)_3$ where R = H, Ph, Mes (Mes = Mesityl)) or $^{H,Cy}LH_6$ = $1,3,5\text{-}C_6H_9(NHPh\text{-}o\text{-}NH_2)_3$ with added pyridine or tertiary phosphine coligands afforded trinuclear complexes of the type $(^{R}L)Mn_3(py)_3$ and $(^{R}L)Co_3(PMe_2R')_3$ (R′ = Me, Ph). While the sterically less encumbered ligand varieties, ^{H}L or ^{Ph}L, give rise to local square-pyramidal geometries at each of the bound metal atoms, with four anilides forming an equatorial plane and an exogenous pyridine or phosphine in the apical site, the mesityl-substituted ligand (^{Mes}L) engenders local tetrahedral coordination. Both the neutral Mn_3 and Co_3 clusters feature $S = {}^1/_2$ ground states, as determined by direct current (dc) magnetometry, ^1H NMR spectroscopy, and low-temperature electron paramagnetic resonance (EPR) spectroscopy. Within the Mn_3 clusters, the long internuclear Mn−Mn separations suggest minimal direct metal−metal orbital overlap. Accordingly, fits to variable-temperature magnetic susceptibility data reveal the presence of weak antiferromagnetic superexchange interactions through the bridging anilide ligands with exchange couplings ranging from $J = -16.8$ to -42 cm^{-1}. Conversely, the short Co−Co interatomic distances suggest a significant degree of direct metal−metal orbital overlap, akin to the related Fe_3 clusters. With the Co_3 series, the $S = {}^1/_2$ ground state can be attributed to population of a single molecular orbital manifold that arises from mixing of the metal- and *o*-phenylenediamide (OPDA) ligand-based frontier orbitals. Chemical oxidation of the neutral Co_3 clusters affords diamagnetic cationic clusters of the type $[(^{R}L)Co_3(PMe_2R)_3]^+$. Density functional theory (DFT) calculations on the neutral ($S = {}^1/_2$) and cationic ($S = 0$) Co_3 clusters reveal that oxidation occurs at an orbital with contributions from both the Co3 core and OPDA subunits. The predicted bond elongations within the ligand OPDA units are corroborated by the ligand bond perturbations observed by X-ray crystallography.

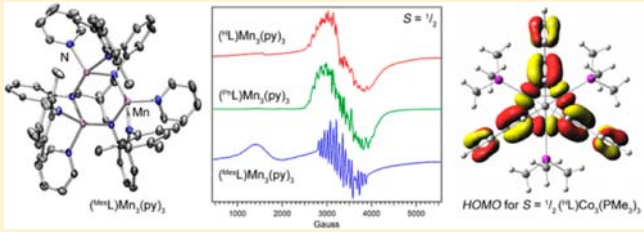

A. INTRODUCTION

Open-shell polynuclear clusters that feature close (ca. < 3 Å) M−M separations are utilized extensively in biology. Aside from the carbonyl/cyanide supported Fe-only hydrogenases,[1] nearly all of the polynuclear metallocofactors feature an open-shell electronic configuration. These clusters are used to mediate electron transfer ($[Fe_2S_2]$ ferrodoxins, $[Fe_4S_4]$ clusters, and $[Fe_3S_4]$ aconitase),[2] reduction chemistry (FeMo, VFe, and Fe-only nitrogenases;[3] Cu_Z site in nitrous oxide reductase[4]), and oxidation chemistry (Mn−O cluster in oxygen-evolving complex in photosystem II;[5] Cu- and Fe-containing clusters in particulate[6] and soluble[7] methane monooxygenase, respectively). In an attempt to realize structural and functional models of these cofactors, researchers have utilized synthetic inorganic chemistry to prepare polynuclear molecular clusters where the protein superstructure has been replaced by organic ligands. However, the majority of ligands that support cluster formation induce low-spin configurations, often precluding the reactivity exhibited by native metalloenzymes.[8]

To synthesize open-shell cluster complexes meeting the aforementioned structural criteria, one can envision use of a flexible, multinucleating ligand composed of weak-field binding sites to direct the formation of predesigned multinuclear architectures. In addition to synthetic tunability, this directed approach offers the distinct advantage of the ability to probe how the ligand scaffold influences the overall molecular symmetry and electronic structure. Toward this end, we recently reported the trinucleating platform, $^{H}LH_6$,[9] and its ability to direct the formation of trigonal planar Fe_3[9] and octahedral Fe_6[10] clusters, where steric modifications to the ligand platform have resulted in dramatic changes to the electronic structure (where ^{R}L = $MeC(CH_2NPh\text{-}o\text{-}NR)_3$; R =

Received: June 17, 2012
Published: September 19, 2012

Scheme 1

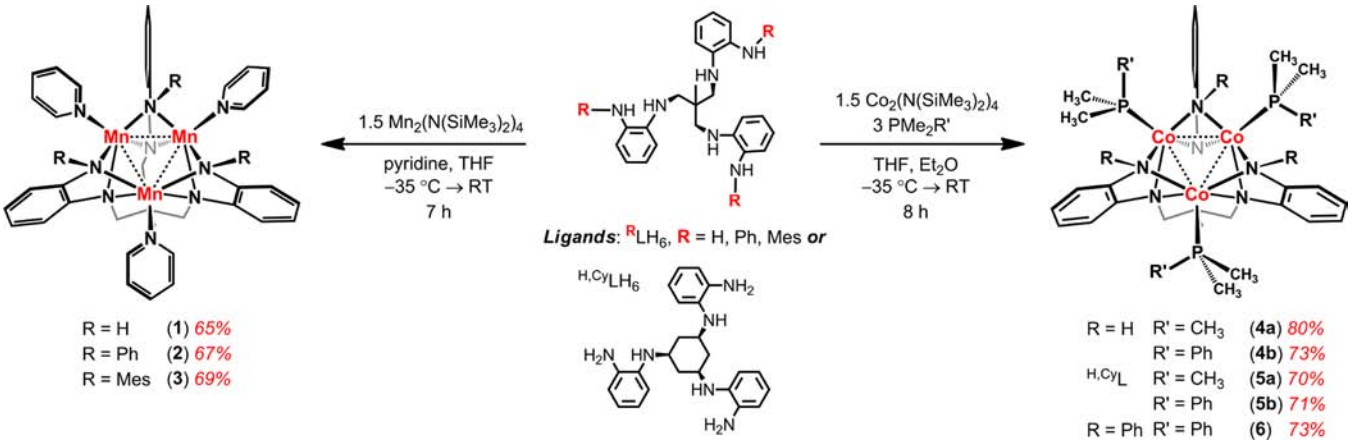

H,[9] Ph,[11] $SiMe_2tBu$[12]). For instance, the proton-capped ligand ($^{H}L^{6-}$) permits close metal−metal contacts giving rise to a low-spin ground state ($S = 1$) for $(^{H}L)Fe_3(PMe_2R)_3$.[9] Appendage of large substituents onto the ligand's peripheral anilide units gives rise to clusters with much larger spin ground states (i.e., $S = 6$ for $(^{Ph}L)Fe_3(thf)_3$,[11] $(^{tbs}L)Fe_3(thf)$;[12] thf = tetrahydrofuran). Importantly, the open-shell configurations present in the Fe_3 clusters have led to facile reactivity with small molecule substrates. For example, reaction of the $S = 6$ complex $(^{tbs}L)Fe_3(thf)$ was shown to activate azide to afford the cluster $[(^{tbs}L)Fe_3(\mu^3\text{-}N)]^-$.[12] Given these initial results with iron, we sought to extend this methodology to include other 3d transition metals, to probe the correlation between molecular and electronic structure as a function of ligand type and transition metal employed.

Following a synthetic approach similar to that used for the trinuclear iron complexes, we present herein trinuclear complexes featuring divalent Mn and Co. Within this family of compounds, different ligand architectures give rise to different molecular symmetries. Following the successful expansion of our synthetic protocols to include Mn, Fe, and Co polynuclear complexes, this report will be directed toward addressing the following questions: (1) How does the overall molecular symmetry impact the electronic structure? (2) To what extent do the redox-active ligand components participate in the observed redox behavior characteristic of the trinuclear clusters? (3) What governs the nature of coupling between the metal centers in the trinuclear complexes?

B. RESULTS

B.1. Synthesis of $^{Mes}LH_6$ and M_3 Clusters. We have used hexadentate aniline-based ligands to assemble tri- and hexanuclear metal cores in the same proximal space.[9−11] The synthesis of the ligand platforms $MeC(CH_2NHPh\text{-}o\text{-}NH_2)_3$ ($^{H}LH_6$),[9] $1,3,5\text{-}C_6H_9(NHPh\text{-}o\text{-}NH_2)_3$ ($^{H,Cy}LH_6$),[12] $MeC(CH_2NHPh\text{-}o\text{-}NHPh)_3$ ($^{Ph}LH_6$)[11] have recently been reported by our group. Introducing phenyl substituents onto the peripheral anilide of the base $^{H}LH_6$ platform dramatically affected the ground state electronic structure observed within the trinuclear iron clusters.[11] Modification of the $^{H,Cy}LH_6$ to include large dimethyl-*tert*-butyl silyl substituents, affording $^{tbs}LH_6$, changed both the electronic structure of the resulting trinuclear complexes as well as the local metal ion binding geometry.[12] To generate a ligand featuring even larger aryl substituents, $^{H}LH_6$ was arylated with mesitylbromide using standard Pd cross-coupling methodologies (2.2% $Pd_2(dba)_3$, 6.6% rac-BINAP, 3.1 equiv of bromomesitylene, 4 equiv of NaO^tBu, toluene, 70 °C for 18 h) to afford the ligand derivative $MeC(CH_2NHPh\text{-}o\text{-}NH(2,4,6\text{-}Me_3C_6H_2))_3$ ($^{Mes}LH_6$) in 72% isolated yield.

Metalation of the ligand platforms was effected via transamination from the metal amide starting materials ($M_2(N(SiMe_3)_2)_4$, M = Mn, Co).[13] For example, addition of 1.5 equiv of $Mn_2(N(SiMe_3)_2)_4$ to $^{R}LH_6$ and excess pyridine in tetrahydrofuran (thf) at −35 °C, followed by standing in a mixture of thf and hexanes at −35 °C, afforded the trinuclear complexes $(^{H}L)Mn_3(py)_3$ (**1**, 65%), $(^{Ph}L)Mn_3(py)_3$ (**2**, 67%), and $(^{Mes}L)Mn_3(py)_3$ (**3**, 69%) as ^{1}H NMR silent, light yellow, crystalline products, akin to the previously reported complex $(^{H}L)Mn_3(thf)_3$.[14] Note that complete transamination to the larger $^{Mes}LH_6$ required heating to 75 °C for 12 h, as confirmed by monitoring $HN(SiMe_3)_2$ evolution by ^{1}H NMR spectroscopy.

Installation of cobalt into the ligand scaffolds followed a similar protocol, where use of the tertiary phosphines PMe_2R (R = Me, Ph) in place of pyridine was necessary to generate isolable species. Specifically, reaction of $^{R}LH_6$ with 1.5 equiv of $Co_2(N(SiMe_3)_2)_4$ and three equiv of PMe_2R (R = Me or Ph) in thf at −35 °C afforded the stable tricobalt complexes $(^{H}L)Co_3(PMe_2R)_3$ (R = Me (**4a**, 80%) or Ph (**4b**, 73%)), $(^{H,Cy}L)Co_3(PMe_2R)_3$ (R = Me (**5a**, 70%) or Ph (**5b**, 71%)), and $(^{Ph}L)Co_3(PMe_2Ph)_3$ (**6**, 73%) as dark red-brown solids in good isolated yields (see Scheme 1). Each of the Co_3 clusters shows a well-defined paramagnetically shifted ^{1}H NMR spectrum, typically exhibiting the appropriate number of proton resonances for complexes of C_3 symmetry. Addition of only 2 equiv of PMe_2Ph in the reaction of 1.5 equiv of $Co_2(N(SiMe_3)_2)_4$ with $^{Ph}LH_6$ afforded a new product that lacks C_3 symmetry, as assayed by ^{1}H NMR and electron paramagnetic resonance (EPR) spectroscopy. Connectivity of this new species, $(^{Ph}L)Co_3(PMe_2Ph)_2$ (**7**, 54%), was confirmed by X-ray crystallography.

B.2. Structures of M_3 Clusters. Crystals suitable for X-ray diffraction analysis of the Mn_3 clusters were grown from standing concentrated solutions in mixtures of thf, hexanes, and pyridine at −35 °C. Complexes **1** and **2** exhibit the same ligand binding modes as previously reported for the $(^{H}L)Fe_3(PMe_2R)_3$ redox series.[9] Here, all six ligand anilides bridge two Mn ions ($6\text{-}\mu^2$), giving rise to a local square-pyramidal coordination environment about each metal, where a pyridine occupies the

dx.doi.org/10.1021/ic301278m | *Inorg. Chem.* 2012, 51, 10290−10299

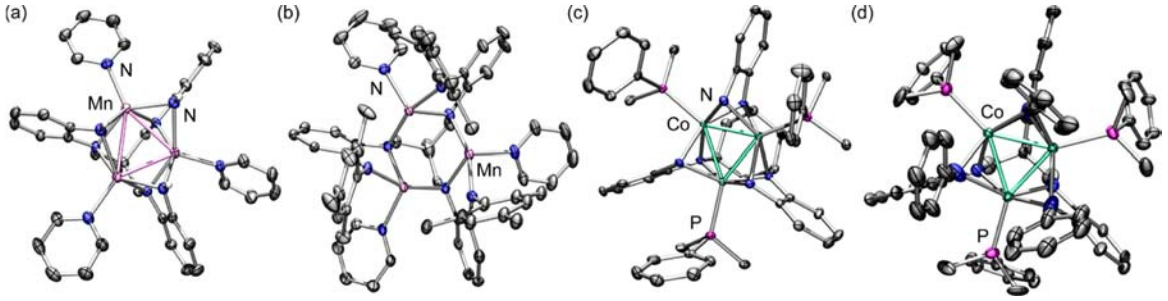

Figure 1. Solid-state structures for $(^{H}L)Mn_3(py)_3$ **1** (a), $(^{Mes}L)Mn_3(py)_3$ **3** (b), $(^{H,Cy}L)Co_3(PMe_2Ph)_3$ **5b** (c), and $(^{Ph}L)Co_3(PMe_2Ph)_3$ **6** (d), with thermal ellipsoids set at the 50% probability level. Hydrogen atoms are omitted for clarity; Mn pink, Co aqua-green, C gray, N blue, P magenta. Selected mean interatomic distances (Å) for **1**: Mn1−Mn2 2.9117(4), Mn1−Mn3 2.8665(4), Mn2−Mn3 2.8650(4), Mn−$N_{base,avg}$ 2.2062(7), Mn−NH_{avg} 2.1902(7), Mn−$N_{py,avg}$ 2.186(2); **3**: Mn1−Mn2 3.1365(9), Mn1−Mn3 3.1045(11), Mn2−Mn3 3.1371(10), Mn−$N_{base,avg}$ 2.132(2), Mn−$NMes_{avg}$ 2.088(2), Mn−$N_{py,avg}$ 2.220(5); **5b**: Co1−Co2 2.3978(7), Co1−Co3 2.3886(7), Co2−Co3 2.3702(7), Co−$N_{base,avg}$ 2.021(4), Co-NH_{avg} 2.010(5), Co−P_{avg} 2.2302(13); **6**: Co1−Co2 2.4265(17), Co1−Co3 2.4272(18), Co2−Co3 2.4274(18), Co−$N_{base,avg}$ 1.987(8), Co-NPh_{avg} 2.149(9), Co−P_{avg} 2.253(3).

Table 1. Selected Bond Lengths (Å) and Angles (deg) for Complexes 1−3, 4b, 5b[a], 6[a], and 7[a]

	1	2	3	4b	5b	6	7
M1−M2	2.9117(4)	2.8104(4)	3.1365(9)	2.3820(4)	2.3978(7)	2.4265(17)	2.4377(7)
M1−M3	2.8665(4)	2.8542(4)	3.1045(11)	2.3796(4)	2.3886(7)	2.4272(18)	2.3368(7)
M2−M3	2.8560(4)	2.7960(4)	3.1371(10)	2.3965(5)	2.3702(7)	2.4274(18)	2.4385(7)
M1−N1	2.242(2)	2.200(1)	2.124(2)	2.089(2)	1.971(4)	1.988(7)	1.925(3)
M1−N2	2.207(2)	2.183(1)	2.144(2)	2.068(2)	1.999(3)	1.983(8)	1.921(3)
M2−N2	2.187(2)	2.181(1)	2.119(2)	1.979(2)	2.063(3)	1.992(7)	2.053(3)
M2−N3	2.212(2)	2.192(1)	2.139(3)	1.952(2)	2.042(4)	1.989(8)	2.042(3)
M3−N1	2.191(2)	2.188(1)	2.138(2)	1.956(2)	2.024(4)	1.981(7)	1.948(3)
M3−N3	2.187(2)	2.201(1)	2.124(2)	1.975(2)	2.026(3)	1.987(8)	1.984(3)
M1−N4	2.191(2)	2.206(1)	2.099(2)	2.085(2)	1.964(3)	2.174(9)	1.853(3)
M1−N5	2.172(2)	2.311(1)		2.112(2)	1.979(4)	2.120(9)	2.060(3)
M2−N5	2.201(2)	2.300(1)	2.084(3)	1.994(2)	2.027(4)	2.108(9)	2.029(3)
M2−N6	2.189(2)	2.186(1)		1.956(2)	2.060(4)	2.181(8)	2.053(3)
M3−N6	2.196(2)	2.304(1)	2.077(2)	1.958(2)	2.040(3)	2.173(9)	2.017(3)
M3−N4	2.214(2)	2.193(1)		1.990(2)	1.993(4)	2.136(9)	2.185(3)
M1−L1	2.2074(18)	2.1649(15)	2.214(2)	2.2026(6)	2.2358(12)	2.253(3)	
M2−L2	2.1890(19)	2.1489(15)	2.213(3)	2.2298(6)	2.2277(12)	2.252(3)	2.2906(12)
M3−L3	2.1808(18)	2.1647(15)	2.248(4)	2.2309(6)	2.2271(13)	2.253(3)	2.2607(11)
M3−M1−M2	59.44(1)	59.15(1)	60.35(2)	60.44(1)	59.36(2)	60.02(5)	61.38(2)
M3−M2−M1	59.50(1)	61.21(1)	59.32(2)	59.73 (1)	60.13(2)	60.01(5)	61.35(2)
M2−M3−M1	61.06(1)	59.65(1)	60.33(2)	59.83(1)	60.51(2)	59.98(5)	57.27(2)
M2−N1−M3	82.49(6)	79.81(5)	93.50(9)	72.15(6)	73.35(12)	75.57(5)	74.30(11)
M1−N2−M3	80.80(6)	79.33(5)	94.73(10)	74.62(6)	70.87(11)	75.53(5)	74.29(11)
M1−N3−M2	80.09(6)	81.25(5)	94.77(10)	72.45(6)	72.80(11)	75.93(5)	75.76(11)
M2−N4−M3	80.56(6)	77.15(5)		72.15(5)	73.11(12)	67.83(5)	70.59(11)
M1−N5−M3	83.60(6)	76.98(5)		73.96(6)	72.24(12)	67.70(5)	69.95(11)
M1−N6−M2	80.94(6)	78.61(5)		71.43(6)	72.91(12)	67.70(5)	
M−N−M_{avg}	81.43(7)	78.86(6)	94.33(11)	72.29(7)	72.55(13)	71.71(6)	72.98(12)

[a]From representative molecule in asymmetric unit.

apical site, trans to a dimetal unit (see Figure 1 and Supporting Information, Figure S6 for representative structures and Table 1 for selected bond lengths and angles). Unlike the iron congener which exhibits very close Fe−Fe ion separation (d_{Fe-Fe} 2.299(2) Å), the average Mn−Mn separation in **1** (2.8550(5) Å) and **2** (2.8201(5) Å), like $(^{H}L)Mn_3(thf)_3$ previously reported,[14] exceeds the van der Waals radius of Mn,[15] suggesting little or no direct Mn−Mn interaction. Unlike **1** and **2**, the steric bulk provided by the mesityl groups in **3** alters the local Mn coordination geometry. In particular, the three peripheral anilides no longer bridge adjacent metal sites giving rise instead to tetrahedral coordination at each Mn (see Figure 1b). This steric bulk also enforces even greater Mn−Mn separation (3.1252(7) Å), although the overall molecular C_3-symmetry is preserved. The range of Mn−Mn separations found in compounds **1**−**3** are similar to previously reported polynuclear Mn^{II} clusters.[16,17]

Crystals suitable for X-ray diffraction analysis of the Co_3 clusters were grown from concentrated hexane solutions at ambient temperature (**4a**,**b**) or via slow evaporation of benzene solution (**5a**,**b**, **6**, and **7**). Representative molecular structures are shown in Figure 1, and selected bond lengths and angles are listed in Table 1. In agreement with the respective ^{1}H NMR spectra, the molecular structures of **4**−**6** confirm the C_3-

dx.doi.org/10.1021/ic301278m | Inorg. Chem. 2012, 51, 10290−10299

symmetry, and, like complexes **1** and **2**, each of the cobalt atoms are bridged by four anilide units from the ligand. Each of the three cobalts reside in a distorted square pyramid that consists of four bridging anilides forming an equatorial plane, with the ancillary phosphine occupying the apical site, *trans* to a dicobalt unit. The average Co−Co separations (**4b** 2.3860(5) Å, **5b** 2.3855(8) Å) show little variation with changing the tris-anilide backbone (^{H}L vs ^{H,Cy}L) and are longer than those in the isostructural iron congener (^{H}L)Fe$_3$(PMe$_2$R)$_3$ (average Fe−Fe distances are 2.299(2) Å).[9] In contrast, the Co−Co separation for the ^{Ph}L ligand variant in **6** (2.4270(19) Å) is contracted from the iron congener (^{Ph}L)Fe$_3$(PMe$_2$Ph)$_3$ (2.5853(14) Å).[11] Although the average Co−Co separation in **6** is elongated by ∼0.04 Å relative to **4b** and **5b**, the average distance is not beyond the van der Waals contact radius and is therefore consistent with metal−metal bonding interactions.[15] The Co−Co interatomic distances are similar to those reported for trigonal cobalt cyclopentadienyl clusters,[18] likely arising from overlap of metal-based σ and π orbitals (vide infra), akin to what has been previously proposed in trigonal Co$_3$ clusters.[19]

The presence of only two bound PMe$_2$Ph ligands in the crystal structure of **7** leads to a distinct coordination environment for each cobalt center and a loss of molecular C_3-symmetry. Two of the peripheral phenyl-anilides bridge adjacent metal sites in a μ^2-fashion, while the third terminally binds Co3 only (see Figure 2). While Co1 retains the square-pyramidal coordination observed in **6**, Co2 is bound by three anilides and one phosphine ligand in a distorted tetrahedral geometry (neglecting M−M interactions). Finally, Co3 resides in a distorted square planar environment that consists solely of four anilides from the (^{Ph}L) ligand. Overall, this asymmetric ligand binding motif results in a significant distortion of the Co−Co separation relative to **6** (see Figure 2 inset). The Co1−Co3 distance is shortened to 2.3371(7) Å, 0.100(1) Å shorter than the Co1−Co2 and Co2−Co3 separations of 2.4377(7) and 2.4385(7) Å, respectively. The Co1−N4 distance (1.853(3) Å) is contracted relative to its bridging counterparts (Co−N$_{Ph}$ (avg) = 2.045(3) Å).

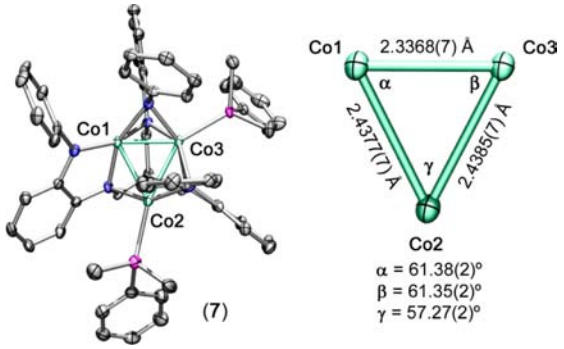

Figure 2. Solid-state structure for (^{Ph}L)Co$_3$(PMe$_2$Ph)$_2$ **7** (thermal ellipsoids set at the 50% probability level; hydrogen atoms are omitted for clarity; Co aqua-green, C gray, N blue, P magenta).

B.3. Spectroscopic Characterization of Neutral M$_3$ Clusters. The X-band EPR spectra for the Mn$_3$ clusters **1**−**3** show strong transitions at 295 K, manifested as simple isotropic signals near g = 2.0, but exhibit fine structure when cooled to 3 K (see Figure 3a). Indeed, each of the spectra at low temperature exhibit substantial hyperfine coupling, presumably to the $I = {}^5/_2$ ^{55}Mn nucleus and potentially to the I = 1 ^{14}N nucleus. Complexes **1** and **2** show spectra exceeding the 16-line pattern expected for hyperfine coupling to all three Mn nuclei ($2nI$ + 1; $A_{\|}$ = 118 MHz for **2** at 77 K; see Supporting Information, Figure S1). In contrast, the spectrum for complex **3** shows a clean 16-line pattern ($A_{\|}$ 182 MHz, g = 2.04, see Figure 2a), despite exhibiting the largest Mn−Mn separation in the series of **1**−**3**. The 16-line pattern, however, likely arises because of coupling of a single Mn center with N nuclei in different environments, though attempts to model the data using either coupling mechanism have failed to reproduce the spectrum obtained. The prominent transition centered at $g \approx$ 4.6 may correspond to a spin-allowed transition associated with the $S = {}^3/_2$ excited state, which may exhibit some thermal population even at 3 K (vide infra). Note that the magnitude of the ^{55}Mn hyperfine coupling is similar to related Mn^{II} clusters (e.g., Mn$_6$(μ^3-NPh)$_4$Br$_4$(thf)$_6$) that have been reported previously.[16d]

To probe the magnetic behavior of the Mn$_3$ clusters, variable-temperature dc susceptibility data were collected in the temperature range of 5−300 K. The resulting plots of $\chi_M T$ vs T for complexes **1**−**3** are shown in Figure 3b. At 300 K, $\chi_M T$ = 3.88, 2.99, and 5.20 cm^3 K/mol for **1**, **2**, and **3**, respectively. All three values are lower than the expected value of 13.1 cm^3·K/

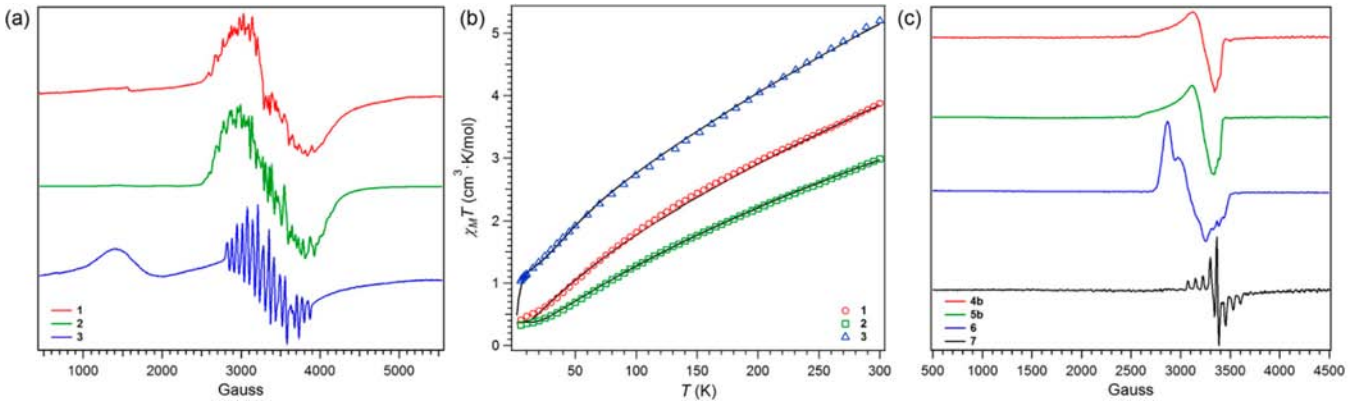

Figure 3. (a) Frozen toluene EPR spectra for (^{H}L)Mn$_3$(py)$_3$ **1** (red), (^{Ph}L)Mn$_3$(py)$_3$ **2** (green), and (^{Mes}L)Mn$_3$(py)$_3$ **3** (blue) obtained at 3 K (X-band, 9.380 GHz). (b) Variable-temperature dc magnetic susceptibility data for (^{H}L)Mn$_3$(py)$_3$ **1** (red circles), (^{Ph}L)Mn$_3$(py)$_3$ **2** (green squares), and (^{Mes}L)Mn$_3$(py)$_3$ **3** (blue triangles), collected in an applied field of 0.5 T. Solid black lines represent simulations using the parameters provided in the text. (c) Frozen toluene EPR spectra for (^{H}L)Co$_3$(PMe$_2$Ph)$_3$ **4b** (red), (^{H,Cy}L)Co$_3$(PMe$_2$Ph)$_3$ **5b** (green), (^{Ph}L)Co$_3$(PMe$_2$Ph)$_3$ **6** (blue), and (^{Ph}L)Co$_3$(PMe$_2$Ph)$_2$ **7** (black) obtained at 3 K (X-band, 9.393 GHz).

dx.doi.org/10.1021/ic301278m | *Inorg. Chem.* 2012, 51, 10290−10299

Scheme 2

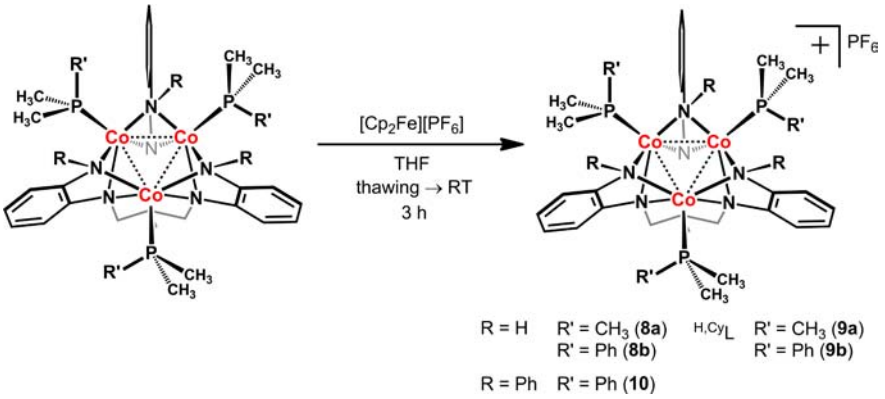

mol for three magnetically isolated $S = {}^5/_2$ Mn^{II} centers (g = 2.00), indicative of antiferromagnetic coupling between Mn^{II} nuclei. As the temperature is lowered, $\chi_M T$ steadily decreases to a minima at 5 K of 0.408, 0.326, and 1.03 $cm^3 \cdot K/mol$ for **1**, **2**, and **3**, respectively, close to the value of 0.375 $cm^3 \cdot K/mol$ expected for an $S = {}^1/_2$ ground state.

Despite the approximate C_3 symmetry **1**–**3**, the $\chi_M T$ vs T data are poorly modeled using MAGPACK[20] according to the following spin Hamiltonian, which assumes an equilateral triangular arrangement of spins and one unique coupling constant (J):

$$\hat{H} = -2J(\boldsymbol{S}_{Mn1}\boldsymbol{S}_{Mn2} + \boldsymbol{S}_{Mn2}\boldsymbol{S}_{Mn3} + \boldsymbol{S}_{Mn1}\boldsymbol{S}_{Mn3}) + g\mu_B\boldsymbol{S}\cdot\boldsymbol{B} \quad (1)$$

Rather, the data can be successfully modeled according to the following spin Hamiltonian considering an isosceles triangle, where two distinct coupling constants are employed:

$$\hat{H} = -2[J_1(\boldsymbol{S}_{Mn1}\boldsymbol{S}_{Mn2} + \boldsymbol{S}_{Mn2}\boldsymbol{S}_{Mn3}) + J_2\boldsymbol{S}_{Mn1}\boldsymbol{S}_{Mn3}] + g\mu_B\boldsymbol{S}\cdot\boldsymbol{B} \quad (2)$$

Note that data for a related anilido-bridged Mn_3 cluster with an $S = {}^1/_2$ ground state have been modeled analogously.[16f] Moreover, closer inspection of the Mn–Mn separation in **1** reveals an asymmetry consistent with this formulation, which features two short and one long Mn–Mn distances (Mn1–Mn2 2.8229(4) Å, Mn1–Mn3 2.8155(4) Å, with Mn2–Mn3 2.9267(5) Å). Modeling the data accordingly provides exchange coupling constants of $J_1 = -35(1)$ and $J_2 = -27(1)$ cm^{-1} (g = 2.00(2)) for **1**, $J = -49(2)$ and $J_2 = -39(1)$ cm^{-1} (g = 1.99(3)) for **2**, and $J = -29.5(6)$ and $J_2 = -17.5(3)$ cm^{-1} (g = 2.00(3)) for **3**. These values are considerably larger than those reported for related trigonal carboxylate- and amido-bridged Mn^{II} clusters, which exhibit $J = -0.59$ to -2.36 cm^{-1},[21] and $J = -7.0$ to -11.0 cm^{-1},[16f] respectively. Considering all trigonal Mn_3 clusters, the magnitude of antiferromagnetic exchange (J_1, J_2) track somewhat linearly with the Mn–N–Mn bond angle (see Supporting Information, Figure S9), wherein the larger angle corresponds to weaker coupling between the metal centers.[22]

The X-band EPR spectra of the Co_3 clusters **4b**, **5b**, **6**, and **7**, obtained for frozen toluene solutions at 77 K, are shown in Figure 3c. The EPR parameters for **4b** (g = 2.035, 2.283) are similar to those observed for **5b** (g = 2.043, 2.283). The large deviation from $g = 2$ is a feature that has been observed in other triangular tricobalt complexes.[23] Common to both previously reported examples, as well as to **4b**, **5b**, and **6**, the hyperfine interaction with the ^{59}Co nucleus ($I = {}^7/_2$) is not the sole contributor to the hyperfine observed. Nevertheless, hyperfine coupling to Co is indeed observed in the spectrum of **7**, which displays a well-resolved eight-line pattern ($A_\parallel$ = 68 G, g = 1.988; see Figure 3c), characteristic of a hyperfine interaction with one Co nucleus. One possibility to account for this spectral difference could be the desymmetrization of **7** relative to the trigonally symmetric **6**. As highlighted in Figure 2, the close Co–Co separation of Co1 and Co3 (Co1–Co3 2.3368(7) Å, Co1–Co2 2.4377(8) Å, Co2–Co3 2.4385(7) Å) may indicate greater localization of the unpaired electron on Co2. Despite the difference between the C_3 symmetric species and **7**, each of the complexes show metrical parameters consistent with the same $S = {}^1/_2$ spin state formulation. Benzene solutions of **4**–**7** at 295 K were evaluated by the method of Evans to give solution magnetic moments (μ_B) of 1.79(4) for **4a**, 1.74(6) for **5a**, 1.95(3) for **6**, and 2.02(6) for **7**, indicative of an $S = {}^1/_2$ formulation (1.73 μ_B spin-only) and consistent with the EPR spectra obtained for these complexes.

B.4. Redox Properties of Tricobalt Series. Cyclic voltammograms collected for complexes **1**–**3** all showed a cascade of irreversible oxidation events beginning near −1.2 V vs $[Cp_2Fe]^{+/0}$ (see Supporting Information, Figure S5). Accordingly, chemical oxidation of the Mn_3 clusters gave rise to intractable mixtures of products. In contrast, complex **4a** exhibits several redox waves in the cyclic voltammogram (see Supporting Information, Figure S5), reminiscent of the iron congeners.[9] The primary oxidation event for **4b** occurs at −1.75 V vs $[Cp_2Fe]^{+/0}$ (see Supporting Information, Figure S5), suggesting a highly reducing species for a nominally all Co^{II} trinuclear complex. Chemical oxidation of **4**, **5**, and **6** with ferrocenium hexafluorophosphate resulted in the immediate generation of ferrocene, as ascertained via ^1H NMR, along with concomitant disappearance of the paramagnetic resonances and growth of new diamagnetic products. These spectral observations are consistent with the removal of one electron from each of the clusters to give the oxidized products $[(^RL)Co_3(PMe_2Ph)_3][PF_6]$ (R = Me (**8a**) and Ph (**8b**)), $[(^{H,Cy}L)Co_3(PMe_2R)_3][PF_6]$ (R = Me (**9a**) and Ph (**9b**)), and $[(^{Ph}L)Co_3(PMe_2Ph)_3][PF_6]$ (**10**) (see Scheme 2). Oxidation of the neutral Co_3 clusters to cationic species was nearly quantitative, as assayed by ^1H NMR spectroscopy. In addition, **8**, **9**, and **10** could be isolated in 73–85% yield following crystallization from thf at −35 °C. The ^1H, ^{31}P and ^{13}C NMR spectra of the oxidized complexes displayed the expected resonances for the C_3-symmetric molecules. The visible spectra of the cationic complexes **8b**, **9b**, and **10** do not show any

dx.doi.org/10.1021/ic301278m | Inorg. Chem. 2012, 51, 10290–10299

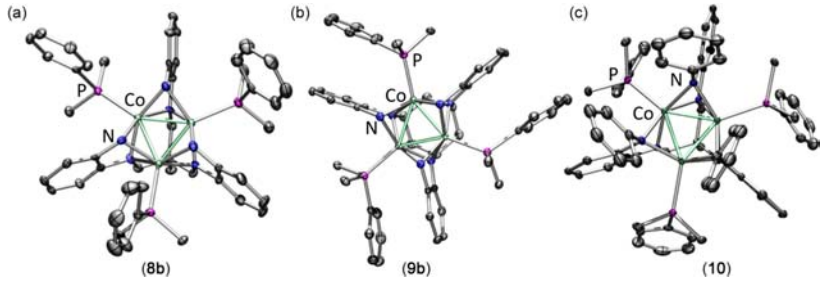

Figure 4. Solid-state structures for $[(^{H}L)Co_3(PMe_2Ph)_3]^+$ **8b** (a), $[(^{H,Cy}L)Co_3(PMe_2Ph)_3]^+$ **9b** (b), and $[(^{Ph}L)Co_3(PMe_2Ph)_3]^+$ **10** (c) with thermal ellipsoids set at the 50% probability level; hydrogen atoms are omitted for clarity; Co aqua-green, C gray, N blue, P magenta). Selected mean interatomic distances (Å) for **8b**: Co1−Co2 2.341(2), Co1−Co3 2.349(2), Co2−Co3 2.342(2), Co−$N_{base,avg}$ 1.957(4), Co−NH_{avg} 1.968(4), Co−P_{avg} 2.235(2); **9b**: Co1−Co2 (Co1−Co3, Co2−Co3) 2.3477(6), Co−$N_{base,avg}$ 1.981(2), Co−NH_{avg} 1.955(2), Co−P 2.2308(7); **10**: Co1−Co2 (Co1−Co3, Co2−Co3) 2.3905(7), Co−$N_{base,avg}$ 1.965(4), Co−NPh_{avg} 2.096(4), Co−P 2.2806(8).

absorption in the region of 650−900 nm that is characteristic of ligand-to-ligand charge transfer bands, commonly associated with the one-electron oxidation of *o*-phenylenediamide ligands to the corresponding monoanionic π-radical *o*-diiminobenzosemiquinonate ligand (see Supporting Information, Figure S4).[24]

The solid-state molecular structures of **8b**, **9b**, and **10** are shown in Figure 4, and selected bond distances and angles are provided in Table 2. The gross structural features of the cationic series are similar to their respective neutral starting materials. Like those in the neutral analogues, the bond metrics within each of the *o*-phenylenediamide ligand branches are characteristic of aromatic, closed-shell dianions (N−C_{Ar} 1.411(10); C_{Ar}−C_{Ar} 1.390(7) Å; Supporting Information, Table S4), unchanged from the precursors and within the error of the measured bond lengths.[24] The Co−N bond distances for the cationic complexes are shorter than those in their respective neutral counterparts. For example, the Co−N_{base} and Co−N_R distances decrease 1.2−3.2% upon oxidation, reflective of the smaller ionic radius for the closed-shell cations relative to the open-shell neutral precursors. Aside from the change in Co−N bond lengths, the metal ion separation in the Co_3 core shows a contraction of similar scale to that observed for $[(^{H}L)Fe_3(PMe_2R)_3]^{+/0}$. The average Co−Co separation also decreases upon oxidation, as exemplified by a contraction in the Co_3 plane of 1.59−3.14% (see Tables 1 and 2), similar in magnitude to that observed in the $[(^{H}L)Fe_3(PMe_2R)_3]^{+/0}$ series (2.19% decrease in the area of the triangular Fe_3 plane).

Table 2. Selected Bond Lengths (Å) and Angles (deg) for Complexes 8b, 9b, and 10

	8b	9b	10
Co1−Co2	2.3406(17)	2.3477(6)	2.3905(7)
Co1−Co3	2.3494(15)		
Co2−Co3	2.3418(17)		
Co1−N1	1.953(4)	1.980(2)	1.962(3)
Co1−N2	1.972(4)	1.981(2)	1.968(3)
Co2−N2	1.960(4)		
Co2−N3	1.960(4)		
Co3−N1	1.952(4)		
Co3−N3	1.947(4)		
Co1−N4	1.964(4)	1.955(2)	2.072(3)
Co1−N5	1.978(4)	1.956(2)	2.119(3)
Co2−N5	1.971(3)		
Co2−N6	1.971(4)		
Co3−N6	1.947(4)		
Co3−N4	1.974(4)		
Co1−P1	2.234(2)	2.2308(7)	2.2806(8)
Co2−P2	2.244(2)		
Co3−P3	2.227(2)		
Co3−Co1−Co2	59.91(5)	60.00(1)	60.0
Co3−Co2−Co1	60.23(3)		
Co2−Co3−Co1	59.86(5)		

B.4. Density Functional Theory (DFT) Analysis of $[(^{H}L)Co_3(PMe_3)_3]^{0/+}$. To further probe the electronic structure of $[(^{H}L)Co_3(PMe_3)_3]^{0/+}$, geometry optimizations with no symmetry restraints were performed on neutral **4** and **7** and cationic **8** (BP86/TZVP/SV(P)),[25,26] using coordinates from the X-ray data as an initial geometry. Comparison of the calculated bond lengths with those determined from X-ray analysis showed good agreement (see Supporting Information, Table S5). The orbital energies for **4** and **8** are presented in Figure 5. The lowest unoccupied molecular orbital in **8** (or the singly occupied molecular orbital in **4**) features both Co and ligand character. The $3a_2$ orbital, pictured in Figure 5b, is composed of a_2-symmetry combinations from the (^{H}L) ligand *o*-phenylenediamide (OPDA) substituents and the a_2 combination of the three Co d_{xy} orbitals. This orbital combination features weak Co−Co π^* overlap and, more significantly, Co−Nσ^* interactions. The calculated bond metrics for neutral **4** and cationic **8** reproduced the decrease in the Co−Co separation and contraction of the Co−N interactions observed crystallographically, resulting from depopulation of the $3a_2$ orbital. While both the frontier orbitals $1a_2$ and 3e feature significant ligand contribution (see Supporting Information, Figure S10), the remaining orbitals feature a larger component of cobalt parentage (see Supporting Information, Figure S10). Despite the prominence of the OPDA contribution to the frontier orbitals in **4a**, a spin density calculation ($\alpha-\beta$) reveals that the primary spin density is located on the three Co ions, where the spin is equally distributed (for $S = {}^1/_2$: Co1 0.25, Co2 0.26, Co3 0.27), with the remainder being ligand-borne (0.22). The spin density plot for **4a** is illustrated in Figure 6a. As suggested by the EPR spectrum of **7**, the lowered symmetry for the diphosphine complex produces two effects: (1) the conjugation between the OPDA subunits and the trinuclear core frontier orbitals is disrupted, and (2) the lowered symmetry and isosceles distortion of the trinuclear core suggests that the resultant spin is more localized on a single Co center (Co2 in Figure 2). The calculated spin density for **7** corroborates this

dx.doi.org/10.1021/ic301278m | *Inorg. Chem.* 2012, 51, 10290−10299

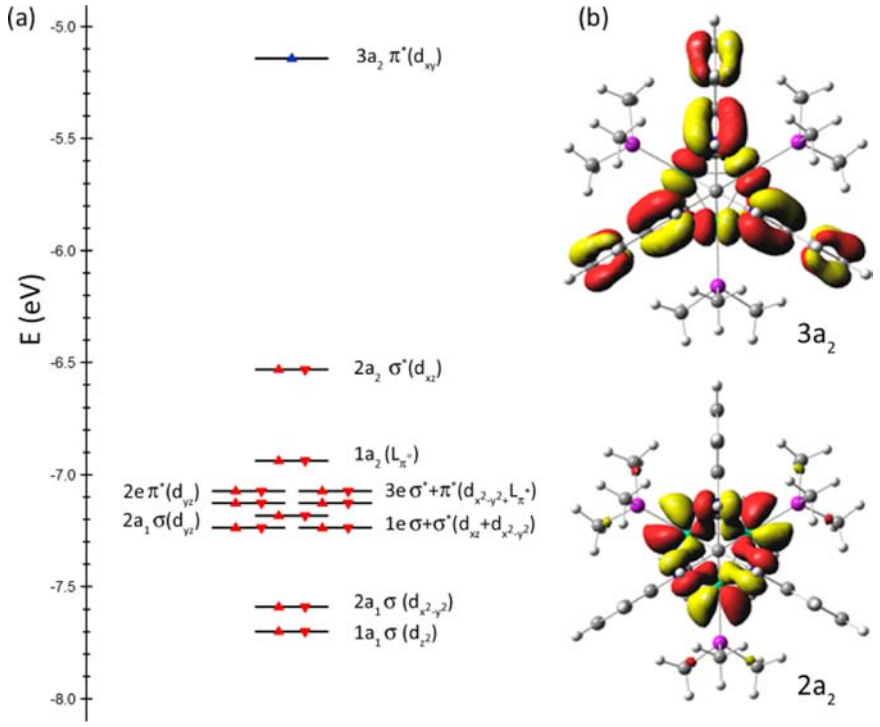

Figure 5. (a) Computed orbital energies for $(^{H}L)Co_3(PMe_3)_3$ (**4a**) and $[(^{H}L)Co_3(PMe_3)_3]^+$ (**8a**). (b) Molecular orbital representations for lowest unoccupied molecular orbital (LUMO, $3a_2$) and highest occupied molecular orbital (HOMO, $2a_2$) in **8a**.

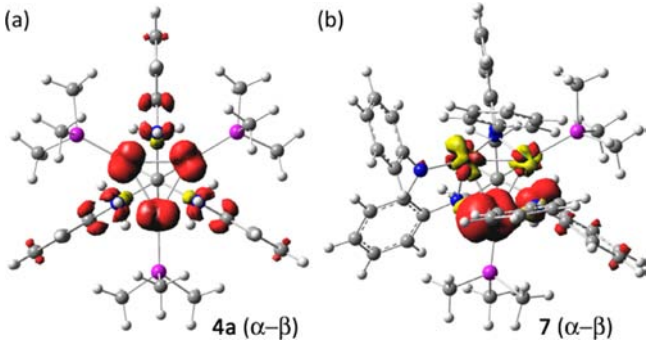

Figure 6. Computed spin density (α–β) plots for **4a** (a) and **7** (b).

assignment (for $S = {}^1/_2$: Co1 −0.01, Co2 0.94, Co3 −0.01), which is illustrated in Figure 6b.

C. DISCUSSION

With the successful expansion of our synthetic approach to include Mn, Fe, and Co polynuclear complexes, several observations require address: (1) How does the overall molecular symmetry impact the molecular electronic structure? (2) To what extent do the redox-active ligand components participate in the observed redox behavior of the clusters? (3) What governs the nature of coupling between the metal ions in the trinuclear complexes? These questions will act as guideposts as we set out to elucidate the correlation between molecular and electronic structure.

C.1. Structural Considerations and Molecular Symmetry. The polynuclear clusters employing the hexadentate ligand $[^{H}L]^{6-}$ and its derivatives fall into three structure types, shown in Scheme 3, where the primary distinguishing characteristic of the structure types can be defined as the variation of angle between the planes defined by the M_3 core

Scheme 3

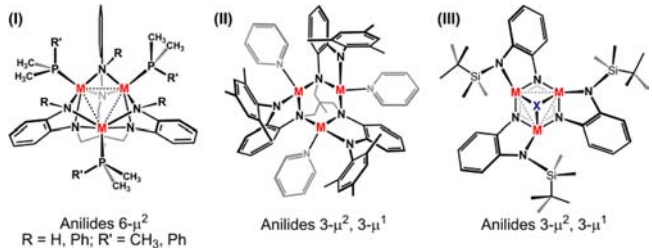

and each of the OPDA planes. In Type I structures, all six anilide groups are bridging (6-μ^2) and the two planes are nearly orthogonal, with average dihedral angles (deg) 89.04 (**1**), 86.67 (**2**), 89.56 (**4b**), 89.31 (**5b**), 88.91 (**6b**), 88.92 for $(^{H}L)Fe_3(PMe_3)_3$,[9] 89.05 for $(^{Ph}L)Fe_3(thf)_3$).[11] In Type II structures, only three anilides bridge (3-μ^2), and the angle between OPDA and M_3 planes deviates significantly from orthogonality (e.g., 68.25° for **3**). Finally, Type III structures show the greatest deviation (e.g., $[(^{tbs}L)Fe_3(\mu^3\text{-}N)]^-$ 37.54°) and only occur upon bridging of a monatomic ligand to the trinuclear core.[12]

The structural variation arises from the binding motif (μ^1 vs μ^2) of the peripheral anilide group, which changes as a function of the size of the anilide substituent. The proton- (^{H}L) or phenyl-capped (^{Ph}L) ligand varieties permit bridging of the peripheral anilide group to adjacent metal ions (Type I), whereas *o*-substituted aryl (^{Mes}L) and silyl (^{tbs}L) groups engender terminal binding to a single metal center (Types II and III, respectively). The larger substituents do not prevent the peripheral anilide unit from bridging exclusively, rather the substituents impede all three OPDA units from bridging adjacent metals. For example, the silyl-substituted complex $(^{tbs}L)Fe_3(thf)$ features one silylanilide unit bridging two Fe sites (Type II).[12]

dx.doi.org/10.1021/ic301278m | *Inorg. Chem.* 2012, 51, 10290−10299

While the metal ion separation within the trinuclear core is affected by the type of supporting ligand, the M−M separation is more sensitive to the metal bound. Consistent with previously reported polynuclear Mn^{II} complexes,[16,27] complexes **1**−**3** do not feature close Mn−Mn interactions, suggesting an increased bonding interaction within the iron and cobalt analogues.[28] Further, within the trinuclear manganese complexes, the M−M separation is largely unaffected by changing the peripheral ligand anilide substituent from H to Ph. However, incorporation of the larger mesityl anilide units results in a significant increase in the Mn−Mn separation and a change in the local coordination environment at each metal center. Importantly, magnetic data for **1**−**3** can be modeled as stemming from superexchange between Mn^{II} ions through the bridging anilides, suggesting that direct Mn−Mn orbital interactions do not play a significant role in the exchange interactions. Complexes **1**−**3** all feature $S = {}^1/_2$ ground states, where the strength of the superexchange interaction is most sensitive to the Mn−N−Mn angle, with the magnitude of J decreasing with increasing Mn−N−Mn angle (see Supporting Information, Figure S9). This magnetostructural correlation is also manifested in the EPR spectra, where stronger coupling contributes to less resolved hyperfine coupling.

Unlike the Mn_3 clusters, employing larger ligand architectures in the Fe_3 clusters significantly increases Fe−Fe separation, which consequently impacts the resulting electronic structure. For instance, $(^{H}L)Fe_3(PMe_3)_3$, an example of a Type I structure, features an average Fe−Fe separation of 2.229(2) Å and an $S = 1$ ground state.[9] Replacing (^{H}L) with (^{Ph}L) to give $(^{Ph}L)Fe_3(PMe_2Ph)_3$ leads to a dramatic increase in average Fe−Fe separation to 2.585(2) Å and an increase in spin ground state to $S = 2$.[11] Although a similar expansion of the Co ion separation is observed in the tricobalt series (see Table 1), complexes **4**−**7** all feature an $S = {}^1/_2$ ground state. This observation suggests that the N_4P-coordination environment imparts a strong enough ligand field to enforce the Co_3 core into a low-spin regime.

C.2. Electronic Structure Considerations. Given the data for all three sets of trinuclear clusters (Mn, Fe, and Co), spanning three structure types, we sought to establish how the structure type dictates electronic interactions between the redox-active components of the complex, the metal ions, and OPDA substituents. The electronic structure of the Type I Fe_3 electron-transfer series focused exclusively on the M−M interactions in deriving a frontier molecular orbital scheme (Figure 7),[9] analogous to the model first proposed by Cotton to rationalize the M−M bonding interactions within $[Re_3Cl_9(\mu_2\text{-}Cl)_3]^{3-}$.[29] Despite its simplicity, this model correctly predicts the ground spin state ($S = {}^1/_2$) for the neutral Co_3 with a proposed electronic configuration of $[(1a_1)_\sigma{}^2(2a_1)_\sigma{}^2(1e)_\pi{}^4(3a_1)^2(2e)^4(1a_2)_{\sigma^*}{}^2(3e)_{\pi^*}{}^4(4e)_{\sigma^*}{}^1]$, which will thus convert to a singlet ground state upon one-electron oxidation.

The DFT results for the redox pair **4a** and **8a** (and by extension, **5**, **6** and $[(^{H}L)Fe_3(PMe_2R)_3]^{+/0}$) reveal a considerable energetic matching of the metal and ligand-based OPDA orbitals. Two of the three frontier orbitals described in Figure 5 exhibit substantial ligand contribution arising from the OPDA subunits. Specifically, the OPDA orbitals of a_2-symmetry that arise from mixing the π^* orbitals mix with the metal-based orbitals of the same symmetry (d_{xy} in $3a_2$, d_{xz} in $2a_2$ and $1a_2$). The electronic configuration within this orbital manifold reproduces the effects of oxidation exhibited by the conversion

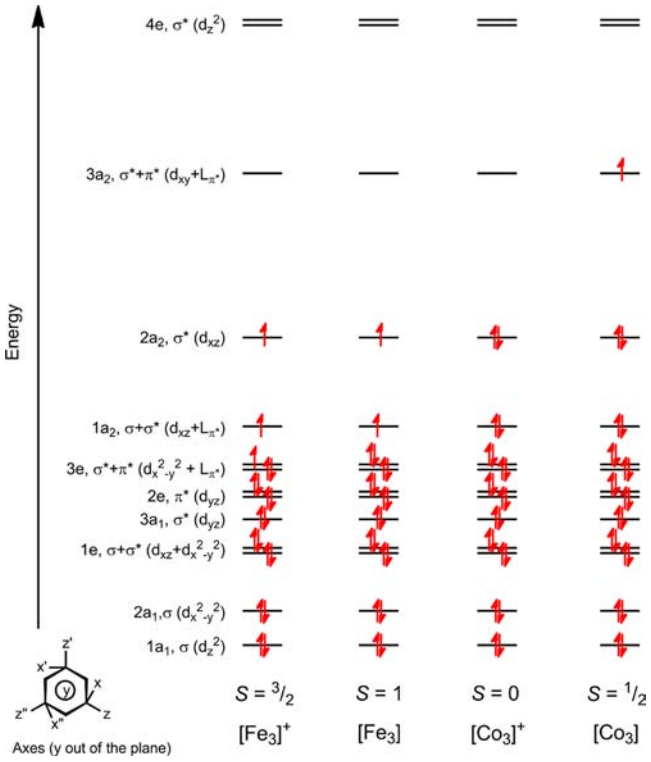

Figure 7. Frontier molecular orbital populations for (from left to right) $[(^{H}L)Fe_3(PMe_2R)_3]^+$ ($S = {}^3/_2$), $(^{H}L)Fe_3(PMe_2R)_3$ ($S = 1$), $[(^{H}L)Co_3(PMe_2R)_3]^+$ ($S = 0$), and $(^{H}L)Co_3(PMe_2R)_3$ ($S = {}^1/_2$).

of **4a** to **8a**. Namely, the Co−Co distances decrease, and subtle structural changes within the OPDA units are also reproduced by the calculation (see Supporting Information, Table S5). This mode of redox activity departs from the traditional electron transfer sequence of *o*-phenylenediamide → benzosemiquinonate → phenylenediimine exhibited by transition metal complexes featuring the redox active fragments.[24] Namely, the one-electron oxidation is borne by the trinuclear M_3 core and all three OPDA subunits. Thus, the traditional charge transfer bands assigned to the OPDA oxidation by Wieghardt and co-workers are either not present,[24c] as in the oxidation of **4**−**6**, or greatly attenuated as observed with $[(^{H}L)Fe_3(PMe_2R)_3]^+$.[9] While the structural changes in the $[(^{H}L)Fe_3(PMe_2R)_3]^{0/+}$ redox series were ascribed to depopulation of an antibonding orbital arising from the interaction of the M-based orbitals, the DFT results indicate the structural contraction arises from the depopulation of an orbital with M−L_N σ^* symmetry ($3a_2$). For the $[(^{H}L)Fe_3(PMe_2R)_3]^{0/+}$ redox pair, the depopulation of an orbital exhibiting M−M σ^* character (3e), in addition to removing electrons from $3a_2$ and $2a_2$, leads to trinuclear core contraction upon oxidation (see Figure 5).

The contribution of the OPDA subunits to the frontier orbitals of Co_3 series is also apparent in the EPR spectra obtained for complexes **4**−**6**. The considerable ligand character in the $S = {}^1/_2$ complexes manifests as broad features in the EPR spectrum without obvious hyperfine coupling to the Co nuclei in the temperature range 4−77 K. However, reducing the molecular symmetry of the Co_3 core in complex **7** effectively disrupts the conjugation of the Co_3 core and OPDA orbitals, thereby localizing the unpaired electron on a single Co center. This localization is evidenced by the sharp 8-line pattern of the EPR spectrum (Co, $I = {}^7/_2$, Figure 2c bottom panel) and is

dx.doi.org/10.1021/ic301278m | Inorg. Chem. 2012, 51, 10290−10299

further corroborated by the geometrical distortion that positions two Co atoms within close proximity of one another (Co1−Co3 2.3368(7) Å) relative to the longer distance to the spin-isolated Co2 (2.4377(7) and 2.4385(7) Å).

A similar phenomenon can be observed in the Mn_3 series. For complexes **1** and **2**, which adopt a Type I structure, the EPR spectra exhibit hyperfine coupling that exceeds the 16-line pattern expected for the coupling to three Mn^{II} ions ($I = {}^5/_2$). This phenomenon may arise because of the coordination mode change of the ligand scaffolds (6-μ^2 vs 3-μ^2, 3-μ^1 anilide ligation), or it may suggest weak mixing of the Mn 3d orbitals with the OPDA subunits. Upon lowering the symmetry to the Type II structure in complex **3** (3-μ^2, 3-μ^1 anilide ligation), the OPDA units are not conjugated to the Mn orbitals of appropriate symmetry, thus the EPR transition exhibits well-defined hyperfine coupling to the Mn and N nuclei, giving a 16-line pattern without obvious contributions from the ligand π-electron framework.

C.3. Comparative Magnetic Coupling within Mn_3, Fe_3, and Co_3 Cores. The M−M interactions observed in the trinuclear complexes investigated changes substantially in moving from Mn to Fe to Co. Indeed, the Mn_3 complexes exhibit coupling exclusively via superexchange through the anilide ligands, with no significant involvement of direct Mn−Mn orbital interactions. While structurally enforcing close Mn^{II}−Mn^{II} contacts can result in bonding interactions,[28] the Mn^{II} centers in complexes **1**−**3** exhibit greater separation. The contrasting behavior of the Mn_3 clusters relative to the Fe_3 and Co_3 analogues may stem from the half-filled 3d orbital shell of the Mn^{II} ion. This electronic configuration represents an energy minimum, thus obviating the need for metal−metal interactions. In contrast, the low-spin Fe_3 and Co_3 complexes do indeed exhibit close M−M separation, within the range where direct M−M orbital overlap is possible. Moreover, calculations performed on the Co_3 series reveal electron delocalization within the frontier orbitals composed of symmetry-allowed interactions between the three Co 3d orbitals. By extension, this description is also appropriate for the Fe_3 series (vide supra). The most significant difference between the Fe_3 and Co_3 series is that the Fe_3 complexes can span both low- and high-spin states ($S = 1 \rightarrow 6$), depending on both supporting (e.g., ^{H}L, ^{Ph}L, ^{tbs}L) and ancillary ligand (e.g., thf, py, PMe_2Ph), while all Co_3 clusters feature low-spin $S = {}^1/_2$ ground states, regardless of the supporting ligand employed. Future ligand permutations will be aimed at accessing more sterically restricted local coordination environments, wherein variable open-shell configurations might be attainable for the Co_3 series.

D. CONCLUSIONS

This work demonstrates that the utility of tris(*o*-phenylenediamine) ligands in directing the formation of trigonal Fe_3 clusters can be extended to manganese and cobalt. A suite of spectroscopic and computational methods was applied to the resulting complexes, and the findings from these investigations are compared to properties previously reported for the Fe_3 analogues to probe the correlation of molecular and electronic structure. Particular attention is paid to the effects of constituent metal identity and steric effects imposed by both supporting and ancillary ligand substitution. Across the entire family of M_3 clusters, three distinct structure types are evident, with the types being primarily defined by the dihedral angle formed by OPDA and M_3 planes. While introduction of bulkier substituents onto the supporting ligand in the Mn_3 clusters can induce a change in structure type, the degree of metal ion separation in Mn_3 and Co_3 clusters is primarily dictated by the metal present in the M_3 core. In addition, while all Mn_3 and Co_3 clusters exhibit an $S = {}^1/_2$ ground state, the ground state arises via different mechanisms: antiferromagnetic superexchange through the anilide ligands for the Mn_3 clusters, and via direct orbital overlap for the low-spin Co_3 clusters. The electronic differences between Co_3 and Mn_3 clusters may stem largely from the d^5 electronic configuration of Mn^{II}, which already resides at an energetic minimum and therefore gains no added stabilization by engaging in metal−metal bonding interactions. The insight gained in this investigation will be employed to direct the formation of new metal clusters derived from poly(OPDA) ligand platforms, with the aim of synthesizing new high-spin, coordinatively unsaturated clusters for cooperative small-molecule activation.

■ ASSOCIATED CONTENT

Ⓢ Supporting Information

Syntheses and spectroscopic data for **1**−**10**; EPR for **1**−**3**, **4b**, **5b**; UV−vis spectra for **4b** and **8b**; CV for **1** and **4a**; X-ray diffraction experimental details for **1**−**10**; comparative bond distances for **1**−**10**; solid-state molecular structures for **2**, **4b**, **8a**; computational details, DFT coordinates, and molecular orbitals for **4a**. This material is available free of charge via the Internet at http://pubs.acs.org.

■ AUTHOR INFORMATION

Corresponding Author

*E-mail: betley@chemistry.harvard.edu.

Notes

The authors declare no competing financial interest.

■ ACKNOWLEDGMENTS

The authors thank Harvard University and the Camille and Henry Dreyfus Fountation (Postdoctoral Program in Environmental Chemistry) for financial support, A.R.F. thanks the NIH for an NIH Ruth L. Kirschstein NRSA fellowship, and T.A.B. is grateful for a George W. Merck fellowship.

■ REFERENCES

(1) (a) Peters, J. W.; Lanzilotta, W. N.; Lemon, B. J.; Seefeldt, L. C. *Science* **1998**, *282*, 1853. (b) Nicolet, Y.; Lemon, B. J.; Fontecilla-Camps, J. C.; Peters, J. W. *Trends Biochem. Sci.* **2000**, *25*, 138. (c) De Lacey, A. L.; Fernández, V. M. *Chem. Rev.* **2007**, *107*, 4304.

(2) Venkateswara Rao, P.; Holm, R. H. *Chem. Rev.* **2004**, *104*, 527 , and references therein.

(3) (a) Peters, J. W.; Stowell, M. H. B.; Soltis, S. M.; Finnegan, M. G.; Johnson, M. K.; Rees, D. C. *Biochemistry* **1997**, *36*, 1181. (b) Mayer, S. M.; Lawson, D. M.; Gormal, C. A.; Roe, S. M.; Smith, B. E. *J. Mol. Biol.* **1999**, *292*, 871. (c) Einsle, O.; Tezcan, F. A.; Andrade, S.; Schmid, B.; Yoshida, M.; Howard, J. B.; Rees, D. C. *Science* **2002**, *297*, 1696.

(4) (a) Brown, K.; Djinovic-Carugo, K.; Haltia, T.; Cabrito, I.; Saraste, M.; Moura, J. J. G.; Moura, I.; Tegoni, M.; Cambillau, C. *J. Biol. Chem.* **2000**, *275*, 41133. (b) Brown, K.; Tegoni, M.; Prudêncio, M.; Pereira, A. S.; Besson, S.; Moura, J. J.; Moura, I.; Cambillau, C. *Nat. Struct. Biol.* **2000**, *7*, 191. (c) Chen, P.; George, S. D.; Cabrito, I.; Antholine, W. E.; Moura, J. G.; Moura, I.; Hedman, B.; Hodgson, K. O.; Solomon, E. I. *J. Am. Chem. Soc.* **2002**, *124*, 744.

(5) (a) Nugent, J. H. A.; Rich, A. M.; Evans, M. C. W. *Biochim. Biophys. Acta, Bioenerg.* **2001**, *1503*, 138. (b) Ferreira, K. N.; Iverson, T. M.; Maghlaoui, K.; Barber, J.; Iwata, S. *Science* **2004**, *303*, 1831. (c) Iwata, S.; Barber, J. *Curr. Opin, Struct. Biol.* **2004**, *14*, 447. (d) Barber, J. *Philos. Trans. R. Soc. London Ser. A* **2007**, *365*, 1007.

(6) Balasubramanian, R.; Rosenzweig, A. C. *Acc. Chem. Res.* **2007**, *40*, 573 , and references therein.
(7) Baik, M.-H.; Newcomb, M.; Friesner, R. A.; Lippard, S. J. *Chem. Rev.* **2003**, *103*, 2385 , and references therein.
(8) (a) Goddard, C. A.; Long, J. R.; Holm, R. H. *Inorg. Chem.* **1996**, *35*, 4347. (b) Chakrabarti, M.; Deng, L.; Holm, R. H.; Münck, E.; Bominaar, E. L. *Inorg. Chem.* **2009**, *48*, 2735. (c) Deng, L.; Bill, E.; Wieghardt, K.; Holm, R. H. *J. Am. Chem. Soc.* **2009**, *131*, 11213.
(9) Zhao, Q.; Betley, T. A. *Angew. Chem., Int. Ed.* **2011**, *50*, 709.
(10) (a) Zhao, Q.; Harris, T. D.; Betley, T. A. *J. Am. Chem. Soc.* **2011**, *133*, 8293. (b) Harris, T. D.; Zhao, Q.; Hernández Sánchez, R.; Betley, T. A. *Chem. Commun.* **2011**, *47*, 6344. (c) Harris, T. D.; Betley, T. A. *J. Am. Chem. Soc.* **2011**, *133*, 13852.
(11) Eames, E. V.; Harris, T. D.; Betley, T. A. *Chem. Sci.* **2012**, *3*, 407.
(12) Powers, T. M.; Fout, A. R.; Zheng, S.-L.; Betley, T. A. *J. Am. Chem. Soc.* **2011**, *133*, 3336.
(13) Anderson, R. A.; Faegri, K., Jr.; Green, J. C.; Haaland, A.; Lappert, M. F.; Leung, W.-P.; Rypdal, K. *Inorg. Chem.* **1988**, *27*, 1782.
(14) Fout, A. R.; Zhao, Q.; Xiao, D.; Betley, T. A. *J. Am. Chem. Soc.* **2011**, *133*, 16750.
(15) Pauling, L. *The Nature of the Chemical Bond*, 3rd ed.; Cornell University Press: Ithaca, NY, 1960; p 403.
(16) (a) Mai, H.-J.; Meyer zu Köcker, R.; Wocadlo, S.; Massa, W.; Dehnicke, K. *Angew. Chem., Int. Ed. Engl.* **1995**, *34*, 1235. (b) Mai, H.-J.; Kang, H.-C.; Wocadlo, S.; Massa, W.; Dehnicke, K. *Z. Anorg. Allg. Chem.* **1995**, *621*, 1963. (c) Mai, H.-J.; Neumüller, B.; Dhnicke, K. *Z. Naturforsch., Teil B* **1996**, *51*, 433. (d) Grigsby, W. J.; Power, P. P. *J. Chem. Soc., Dalton* **1996**, 4613. (e) Alvarez, C. S.; Bond, A. D.; Cave, D.; Mosquera, M. E. G.; Harron, E. A.; Layfield, R. A.; McPartlin, M.; Rawson, J. M.; Wood, P. T.; Wright, D. S. *Chem. Commun.* **2002**, 2980. (f) Hatnean, J. A.; Raturi, R.; Lefebvre, J.; Leznoff, D. B.; Lawes, G.; Johnson, S. A. *J. Am. Chem. Soc.* **2006**, *128*, 14992.
(17) Tsui, E. Y.; Kanady, J. S.; Day, M. W.; Agapie, T. *Chem. Commun.* **2011**, *47*, 4189.
(18) (a) Uchtman, V. A.; Dahl, L. F. *J. Am. Chem. Soc.* **1969**, *91*, 3763. (b) Frisch, P. D.; Dahl, L. F. *J. Am. Chem. Soc.* **1972**, *94*, 5082. (c) Abel, E. W.; Blackmore, T.; Whitley, R. J. *Inorg. Nucl. Chem. Lett.* **1974**, *10*, 941. (d) Madach, T.; Vahrenkamp, H. *Chem. Ber.* **1981**, *114*, 505. (e) Enoki, S.; Kawamura, T.; Yonezawa, T. *Inorg. Chem.* **1983**, *22*, 3821. (f) Colbran, S. B.; Robinson, B. H.; Simpson, J. *Organometallics* **1984**, *3*, 1344. (g) Kubat-Martin, K. A.; Rae, A. D.; Dahl, L. F. *Organometallics* **1985**, *4*, 2221. (h) Bedard, R. L.; Rae, A. D.; Dahl, L. F. *J. Am. Chem. Soc.* **1986**, *108*, 5924. (i) Bedard, R. L.; Dahl, L. F. *J. Am. Chem. Soc.* **1986**, *108*, 5932. (j) Bedard, R. L.; Dahl, L. F. *J. Am. Chem. Soc.* **1986**, *108*, 5942. (k) Barnes, C. E.; Orvis, J. A.; Staley, D. L.; Rheingold, A. L.; Johnson, D. C. *J. Am. Chem. Soc.* **1989**, *111*, 4992.
(19) Strouse, C. E.; Dahl, L. F. *J. Am. Chem. Soc.* **1971**, *93*, 6032.
(20) Borrás-Almenar, J. J.; Clemente-Juan, J. M.; Coronado, E.; Tsukerblat, B. S. *J. Comput. Chem.* **2001**, *22*, 985.
(21) (a) Reynolds, R. A., III; Yu, W. O.; Dunham, W. R.; Coucouvanis, D. *Inorg. Chem.* **1996**, *35*, 2721. (b) Christian, P.; Rajaraman, G.; Harrison, A.; Helliwell, M.; McDouall, J. J. W.; Raftery, J.; Winpenny, R. E. P. *J. Chem. Soc., Dalton Trans.* **2004**, 2550. (c) Lin, W.; Evans, O. R.; Yee, G. T. *J. Solid State Chem.* **2000**, *152*, 152.
(22) (a) Toulouse, G. *Commun. Phys.* **1977**, *2*, 115. (b) Kahn, O. *Molecular Magnetism*; VCH: New York, 1993.
(23) Ebihara, M.; Liba, M.; Kato, M.; Minami, H.; Kawamura, T. *Inorg. Chem. Acta* **2004**, *357*, 533.
(24) (a) Balch, A. L.; Holm, R. H. *J. Am. Chem. Soc.* **1966**, *88*, 5201. (b) Warren, L. F. *Inorg. Chem.* **1977**, *16*, 2814. (c) Chaudhuri, P.; Verani, C. N.; Bill, E.; Bothe, E.; Weyhermüller, T.; Wieghardt, K. *J. Am. Chem. Soc.* **2001**, *123*, 2213. (d) Anillo, A.; Diaz, M. R.; Garcia-Granda, S.; Obeso-Rosete, R.; Galindo, A.; Ienco, A.; Mealli, C. *Organometallics* **2004**, *23*, 471. (e) Bill, E.; Bothe, E.; Chaudhuri, P.; Chlopek, K.; Herebian, K.; Kokatam, S.; Ray, K.; Weyhermüller, T.; Neese, F.; Wieghardt, K. *Chem.—Eur. J.* **2005**, *11*, 204. (f) Chlopek, K.; Bill, E.; Weyhermüller, T.; Wieghardt, K. *Inorg. Chem.* **2005**, *44*, 7087.
(25) Frisch, M. J.; Trucks, G. W.; Schlegel, H. B.; Scuseria, G. E.; Robb, M. A.; Cheeseman, J. R.; Scalmani, G.; Barone, V.; Mennucci, B.; Petersson, G. A.; Nakatsuji, H.; Caricato, M.; Li, X.; Hratchian, H. P.; Izmaylov, A. F.; Bloino, J.; Zheng, G.; Sonnenberg, J. L.; Hada, M.; Ehara, M.; Toyota, K.; Fukuda, R.; Hasegawa, J.; Ishida, M.; Nakajima, T.; Honda, Y.; Kitao, O.; Nakai, H.; Vreven, T.; Montgomery, Jr., J. A.; Peralta, J. E.; Ogliaro, F.; Bearpark, M.; Heyd, J. J.; Brothers, E.; Kudin, K. N.; Staroverov, V. N.; Kobayashi, R.; Normand, J.; Raghavachari, K.; Rendell, A.; Burant, J. C.; Iyengar, S. S.; Tomasi, J.; Cossi, M.; Rega, N.; Millam, N. J.; Klene, M.; Knox, J. E.; Cross, J. B.; Bakken, V.; Adamo, C.; Jaramillo, J.; Gomperts, R.; Stratmann, R. E.; Yazyev, O.; Austin, A. J.; Cammi, R.; Pomelli, C.; Ochterski, J. W.; Martin, R. L.; Morokuma, K.; Zakrzewski, V. G.; Voth, G. A.; Salvador, P.; Dannenberg, J. J.; Dapprich, S.; Daniels, A. D.; Farkas, Ö.; Foresman, J. B.; Ortiz, J. V.; Cioslowski, J.; Fox, D. J. *Gaussian 09*, Revision A.02; Gaussian, Inc.: Wallingford, CT, 2009.
(26) (a) Becke, A. D. *Phys. Rev. A* **1988**, *38*, 3098. (b) Perdew, J. P. *Phys Rev. B* **1986**, *33*, 8822.
(27) (a) Clemente, D. A.; Biagini, M. C.; Rees, B.; Hermann, W. A. *Inorg. Chem.* **1982**, *21*, 3741. (b) Davies, J. I.; Howard, C. G.; Skapski, A. C.; Wilkinson, G. *Chem. Commun.* **1982**, 1077. (c) Creswick, M.; Bemal, I.; Reiter, B.; Hermann, W. A. *Inorg. Chem.* **1982**, *21*, 645. (d) Howard, C. G.; Wilkinson, G.; Thomton-Pett, M.; Hursthouse, M. B. *J. Chem. Soc., Dalton Trans.* **1983**, 2025. (e) Huttner, G.; Schuler, S.; Zsolnai, L.; Gottlieb, M.; Braunwarth, H.; Minelli, M. *J. Organomet. Chem.* **1986**, *299*, 4. (f) Hermann, W. A.; Kneuper, H.-J.; Herdtweck, E. *Chem. Ber.* **1989**, *122*, 433. (g) Kralik, M. S.; Stahl, L.; Arif, A. M.; Stouse, E. D.; Ernst, R. D. *Organometallics* **1992**, *11*, 3617. (h) Mai, H.-J.; Kang, H.-C.; Wocadio, S.; Massa, W.; Dehnicke, K. *Z. Anorg. Allg. Chem.* **1995**, *621*, 1963. (i) Solari, E.; Musso, F.; Gallo, E.; Floriani, C.; Re, N.; Chiesi-Villa, A.; Rizzoli, C. *Organometallics* **1995**, *14*, 2265. (j) Ficker, R.; Hiller, W.; Drobnik, S.; Lorenz, I.-P. *Z. Kristallogr.* **1996**, *211*, 745. (k) Braunschweig, H.; Colling, M.; Hu., C.; Radacki, K. *Angew. Chem., Int. Ed.* **2002**, *41*, 1359. (l) Kheradmandan, S.; Fox, T.; Schmalle, H. W.; Venkatesan, K.; Berke, H. *Eur. J. Inorg. Chem.* **2004**, 3544.
(28) Ashley, A. E.; Cooper, R. T.; Wildgoose, G. G.; Green, J. C.; O'Hare, D. *J. Am. Chem. Soc.* **2008**, *130*, 15662.
(29) (a) Bertrand, J.; Cotton, F. A.; Dollase, W. A. *J. Am. Chem. Soc.* **1963**, *85*, 1349. (b) Cotton, F. A.; Haas, T. E. *Inorg. Chem.* **1964**, *3*, 10.